Chapter 4

Evolution of Magnetic Properties in Ferrites: Trends of Single-Sample and Multi-Sample Sintering

Ismayadi Ismail, Idza Riati Ibrahim and
Rodziah Nazlan

Additional information is available at the end of the chapter

http://dx.doi.org/10.5772/intechopen.68500

Abstract

Microstructure of magnetic materials greatly influences the performance of magnetic properties, and sintering has been used as an agent to tailor the microstructure of these magnetic materials especially ferrites. Nanostructured ferrites prepared by high-energy milling method are often inherently unstable owing to their small constituent sizes, non-equilibrium cation distribution, disordered spin configuration, and high chemical activity. Therefore, sintering of the milled ferrites recrystallizes the nanostructure and causes its transition from an excited metastable (activated) state into the low-energy crystalline state. A better understanding of the response of nanoscale ferrites with changes in temperature is crucial not only for basic science (the development of an atomistic and microscopic theory of the mechanochemical processes) but also because of the technological high-temperature applications in catalysis, ferrofluids and information storage. This chapter discusses on two different sintering schemes, which are a commonly applied multi-sample sintering and a rarely adopted single-sample sintering. Experimental results of single-sample and multi-sample sintering of NiZn ferrites and yttrium iron garnet (YIG) were highlighted, and their microstructural consequences on the magnetic properties were also discussed.

Keywords: microstructural evolution, BH-hysteresis, ferrites, NiZn ferrites, yttrium iron garnet (YIG)

1. Sintering as a microstructure tailoring agent

Microstructure of polycrystalline ceramics is usually complex, consisting of grains, grain boundaries, porosity and secondary phases. This kind of structure is not seen in single crystals. Variations in the microstructure with different kinds of shape, size, distribution and

orientation of the grains play a key role in many of the macroscopic properties including magnetic, thermophysical, mechanical, electrical and many other properties. Essentially, these phenomena are familiar with the polycrystalline ceramics samples having micronic grain size, and the information on their relationships is well understood. Materials in the micrometer scale mostly exhibit physical properties the same as that of bulk form; however, materials in the nanometer scale may exhibit physical properties distinctively different from that of micrometer scale. Nanomaterials may have significantly lower melting point or phase transition temperature and appreciably reduced lattice constants, due to a huge fraction of surface atoms in the total amount of atoms [1]. Materials with an altered 'nano'-microstructure provide potential for new or improved applications [2]. Sintering has been known as an agent to alter the microstructure condition of a polycrystalline material. Through optimization of sintering conditions such as sintering temperature, sintering atmosphere, heating and cooling rates, sintering time and partial pressure of sintering atmosphere, the best materials properties could be achieved. Tailoring the microstructure to attain certain desirable materials properties is the main challenge and of interest in material science.

2. Single-sample and multi-sample sintering

There are two different sintering schemes in producing polycrystalline materials, which are commonly applied multi-sample sintering scheme and rarely adopted single-sample sintering scheme. Generally, reported studies involving sintering and materials properties employed multi-sample sintering scheme [3–9]. The multi-sample sintering has as many starting compacts as the number of the intended sintering temperatures where each sample sintered only once at different temperatures. All compacts are assumed to have identical morphologies, for example, particle size distribution. However, a rarely adopted single-sample sintering scheme has only one single compact with definite starting point and one particular particle size distribution where only one sample sintered at different temperatures. Therefore, multi-sample sintering is subjected to possible statistical errors since the particle size distributions for all the samples may not be as identical as assumed as compared to that of single-sample sintering. Thus, more convincing data could be obtained for the scientific interpretation of the evolution study. Besides, it is more economical with respect to raw materials and sample preparation time. The schematic of the different sintering schemes is been shown in **Figure 1**. Ceramic is defined as the art and science of making and using solid articles [10]. The statement made a clear view that it is not an easy task to produce the same ceramic with almost the same properties because ceramic is composed of a complex system. The question is whether a material scientist is able to make such ceramic by employing single-sample and multi-sample sintering, with almost the same or enhanced properties is of great interest.

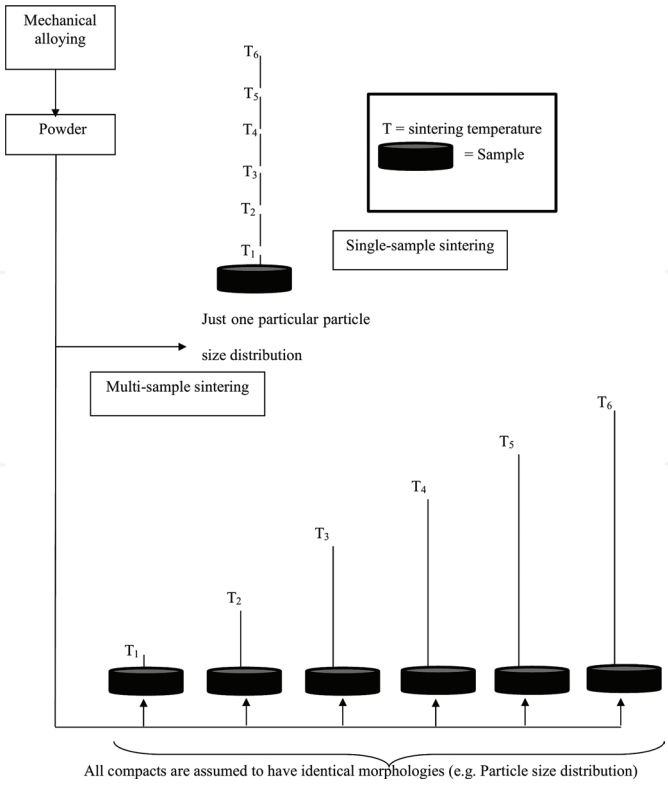

Figure 1. Schematic of different sintering schemes: multi-sample and Single-sample sintering.

3. Magnetic properties evolution and the research gap

Evolution in magnetic properties is laterally correlated with the evolution of the microstructure, particularly from nanometric to micronic regime of grains as shown in **Figure 2**. However, the reported cause and effect sequences, in the magnetic properties research literature, are an experimental sequence focused mainly on yielding the final outcome, for example, the final microstructure-magnetic properties relationship at final sintering temperature. Therefore, microstructural dependence of magnetic properties for polycrystalline ferrite having micrometer grain size has been widely studied and greatly understood. However, research on ferrite from the nanometer scale has been a field of intense study, due to the novel properties shown by particles located in the transition region between the isolated atoms and bulk solids. Their novel properties make them attractive, both from the scientific knowledge of understanding

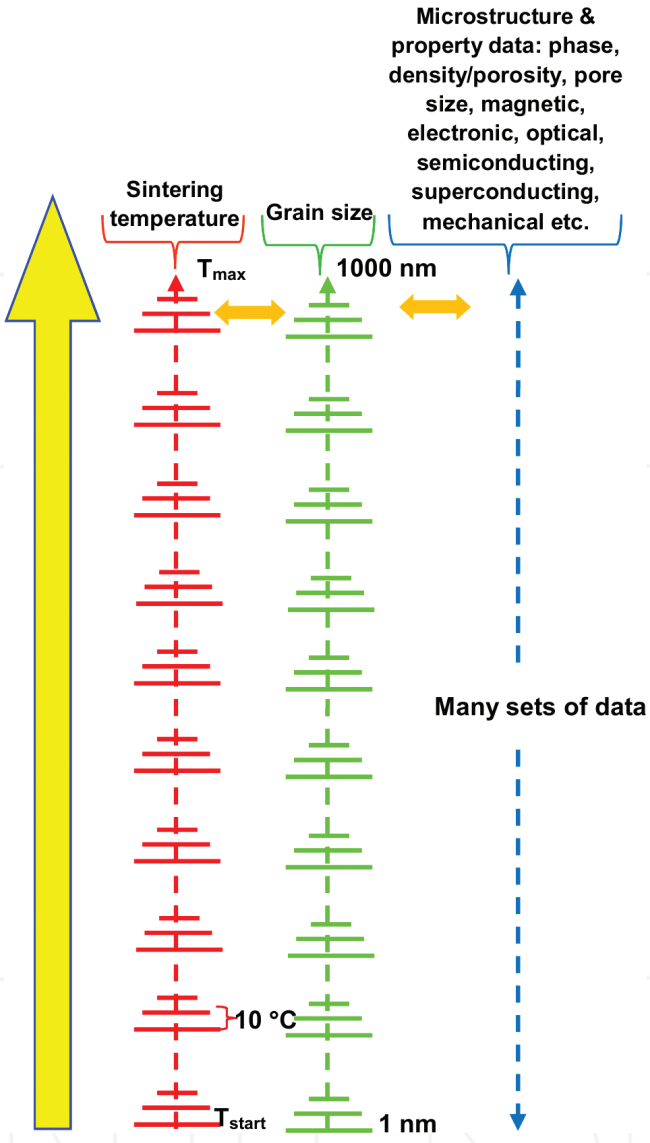

Figure 2. Grand evolution-data acquisition scheme for polycrystalline materials.

their properties, and the technological importance of enhancing the performance of the present materials. A fundamental line of scientific enquiry thus has been neglected, particularly by ferrite researchers for more than 70 years: What would be the magnetic-microstructure relationships at various intermediate sintering conditions during the parallel evolutions of the morphology and magnetic properties? Therefore, much possible essential development information has been neglected, thus reducing the capabilities of producing good fundamental scientific knowledge, which lies behind the parallel evolution of the microstructure-material

properties, particularly in magnetic properties. This absence information has leaving behind many research gaps and research questions that have to be solved in this study:

i. How microstructural properties evolve with the magnetic properties from several nanometers to micrometer grains size?

ii. How the evolution of an amorphous-crystalline mixture state to complete polycrystalline state affects the microstructure-magnetic properties?

iii. Does sample with nanometer grain size demonstrates the similar magnetic properties with samples having micron grain size?

iv. What is the relationship of evolving microstructure properties with magnetic properties of material?

v. When is the remarkable transition of magnetic properties between the nanometer and micrometer grain size?

Hence, revealing the systematic development of grains having size from several nanometers up to micrometer is an important parameter of designing best materials properties. The evolution has yet to be established in wide variation of properties since the knowledge of parallel evolution of microstructure and properties is absence in these materials:

i. Other electroceramics, for example, high-temperature heating elements and electrodes, voltage dependent resistors, thermally sensitive resistors, solid fast-ion conductors, humidity and gas sensors, superconductors

ii. Thermo-mechanical ceramics, for example, SiC, Al_2O_3

iii. Rare-earths-based magnetic materials, for example, $Nd_9Fe_{14}B$, $SmCo_{17}$

iv. Transition metal-alloys based magnetic materials, for example, NiFe, NiCo

v. Mechanical metals and metallic alloys (elemental), for example, pure iron, copper, chromium, nickel/carbon steels

vi. Polycrystalline semiconductors, for example, zinc oxide

4. Introduction to ferrites

Generally, a class of magnetic oxide, which contains iron oxide as a primary component, is commonly described as ferrites. Similar to most ceramic material, the physical properties of ferrite are also hard but brittle. The drastic progress in the development and growth of ferrites for technological application has once force the industry to leave behind the research and study in ferrite. The industrial importance of ferrites becomes apparent when one examines the diversity of their applications. Ferrite has been extensively used in various electronic devices. These applications include choke filters [11], transformers [12], antenna rods [13], microwave devices [14, 15], isolators [16], circulators [17], phase shifters [18] and many others. The frequencies of the applications range from direct current (DC) to the highest one at which any electronic device can function [19].

Ferrite exhibits ferrimagnetic behavior which possesses unequal, anti-parallel ionic magnetic moments resulting in a net moment due to incomplete compensation. There are three classes of commercial ferrite in the industry, and each of the types has their own specific crystal structure. The three classes of the commercial ferrites are as follows:

i. Soft ferrite with spinel cubic structure, for example, nickel zinc ferrite and manganese zinc ferrite.

ii. Soft ferrite with garnet structure, for example, yttrium-based garnets that are used in microwave devices.

iii. Hard ferrite with magnetoplumbite structure, for example, barium hexaferrite and strontium hexaferrite. The hexagonal ferrites develop high coercivity and are an important member of the permanent magnet family.

5. Sintering of ferrite materials

Ferrites are commonly fabricated via two major techniques: the conventional technique and the non-conventional technique. Through the conventional ceramic technique, the raw material powders are mixed and sintered at over 1000°C sintering temperature. This process allows interdiffusion of atoms in a pre-selected composition to form a mixed crystal. The other technique for preparing ferrites is the non-conventional technique. A non-conventional technique in a liquid medium may produce intermediate, finely divided mixed hydroxides or mixed organic salts, which would assist the subsequent diffusion process [20].

Various synthesis methods including the conventional and non-conventional techniques of ferrites preparation have been shown in **Table 1**. The table shows that the formation of ferrite through non-conventional technique could be produced by using the obtained fine powders at much lower sintering temperature. Yet most of the techniques still require sintering, although at relatively lower temperatures to produce a single phase material. The sintering temperature could be as low as 200°C [21], though displaying least performance of magnetic properties compare to much higher sintering temperatures. Highest sintering temperature is normally employed for synthesizing bulk ferrites via solid state reaction and has been shown to produce optimum magnetic properties (see **Table 1**). However, low sintering temperature is required for nano-sized materials as basic requirement since magnetic properties of the bulk materials differ drastically from the nano-sized materials.

Sintering in certain condition of atmosphere would form pure phase as has been observed in reference [22]. Furthermore, sintering atmosphere is also responsible in altering the magnetic properties and the effects can be observed in cation redistribution and oxygen deficiency [21]. The sintering time displays in **Table 1**, which shows that the non-conventional technique requires much shorter sintering time as compare to conventional technique. The right selection of sintering times would result in high densification and homogeneous materials which are largely important in magnetic materials since less densified materials result in hindrance to the domain wall movement, thus reducing the total magnetization. In addition, the

Material	Synthesis method	Starting materials	Sintering conditions	Microstructure features	Optimum magnetic properties	Reference
$Ni_{0.3}Cu_{0.2}Zn_{0.5}Fe_2O_4$	Citrate precursor method	$Fe(NO_3)_3{\cdot}9H_2O$ $Zn(NO_3)_2{\cdot}4H_2O$ $Cu(NO_3)_2{\cdot}3H_2O$ $Ni(NO_3)_2{\cdot}6H_2O$ Citric acid	Sintering atmosphere: air-, argon-, carbon monoxide-ambient atmospheres Sintering temperature: 200,400 and 600°C Sintering time: 2 h	Crystallite sizes increased with increased sintering temperatures for all sintering atmosphere ranging from 22.7 to 28.1 nm for air atmosphere, 8.8–24. 7 nm for argon atmosphere and 10.1–31.6 nm for carbon monoxide-ambient atmosphere	Saturation magnetization, M_s: 69.1 emu/g for sample sintered at 600°C under carbon monoxide-ambient atmosphere	[21]
$NiFe_2O_4$	Sol-gel auto-combustion method	$Fe(NO_3)_3{\cdot}9H_2O$ $Ni(NO_3)_2{\cdot}6H_2O$ Citric acid	Sintering temperature: 900, 1100, 1200 and 1300°C Sintering time: 2 h	Average grain sizes increased from 0.1 to 2.2 μm with increasing sintering temperatures Density increased from 2.93 to 4.30 g/cm^3 with increasing sintering temperatures	M_s: ~50.0 emu/g for sample sintered at 1100°C	[25]
$Ni_{0.5}Zn_{0.5}Fe_2O_4$	Co-precipitation method	$NiCl_2$ $ZnCl_2$ $FeCl_3$ NaOH	Sintering temperature: 800 and 900°C Sintering time: 3 h	Average crystallite sizes increased from 38.4 to 42.2 nm with increasing sintering temperatures	M_s: 89.5 emu/g for sample sintered at 900°C	[26]
$Ni_{0.266}Zn_{0.66}Cu_{0.09}Fe_{1.968}O_{4-\delta}$	Solid-state reaction method	NiO ZnO CuO Fe_2O_3	Sintering atmosphere: Air Sintering temperature: 1050°C Sintering time: 1, 3, 5 and 7 h	Average crystallite sizes increased from 3.9 to 12.9 μm with increasing sintering times Density increased from 5.06 to 5.21 g/cm^3 with increasing sintering times	M_s: 245.1 emu/cm^3 for sample sintered for 7 h Initial permeability, μ_i, at 1 kHz: 2305 for sample sintered for 7 h	[23]

Material	Synthesis method	Starting materials	Sintering conditions	Microstructure features	Optimum magnetic properties	Reference
$Y_3Fe_5O_{12}$	Solid-state reaction method	Fe_2O_3 Y_2O_3	Two different sintering curves Curve 1 Sintering temperatures, T_1:1200–1450°C Sintering time: none Heating rate:10°C/min Cooling rate: 2°C/min Curve 2 Sintering temperatures, T_1:1350°C, T_2:1200 °C T_1:1350°C, T_2:1300 °C T_1:1450 °C, T_2:1300 °C Sintering time at T_2: 6, 12, 18 and 24 h Heating rate:10°C/min Cooling rate: 25°C/min	Sample sintered at T_1:1350°C, T_2:1300°C for 18 h attained the highest relative density (99.1%)	M_s: 27.4 emu/g for sample sintered at T_1 = 1350°C, T_2:1300°C for 18 h	[27]
NiCuZn ferrite	Commercial purchased NiCuZn ferrite powder and sintering	Commercial purchased NiCuZn ferrite	Sintering temperature: 850, 900, 950, 1000 and 1050°C Sintering time: 2 h	Density increased from 4.0 to 4.3 g/cm^3 Average grain sizes increased from 3.0 to 7.5 μm with increasing sintering temperatures	Initial permeability, μ_i, at 5 MHz increased with increased sintering temperature with maximum value of ~112 for sample sintered at 1050°C	[3]
$CoFe_2O_4$	Citrate precursor method	$Co(NO_3)_2.6H_2O$ $Fe(NO_3)_2.9H_2O$ $C_6H_8O_7$	Sintering temperature: 900, 1000 and 1100°C	Average grain sizes increased from 90.0 to 100.0 nm with increasing sintering temperatures	M_s increased from 53.7 emu/g to 74.5 emu/g	[4]

Material	Synthesis method	Starting materials	Sintering conditions	Microstructure features	Optimum magnetic properties	Reference
$Zn_{0.35}Ni_{0.57}Co_{0.03}Fe_{2.05}O_4$	Chemical combustion route	Metal nitrates Citric acid	Sintering temperature: 1050 and 1150°C Sintering time: 1 h	Average grain sizes increased from 0.61 to 0.94 μm with increasing sintering temperatures	Real part of the initial permeability increases with increasing sintering temperature from 85.2 to 209.7 at 10 kHz and from 90.4 to 238.1 at 1 MHz	[28]
$BaFe_{12}O_{19}$	High-energy ball milling	$BaCO_3$ Fe_2O_3	Sintering atmosphere: Air atmosphere Sintering temperature: 800, 900 and 1150°C Sintering time: 1 h	The highest measured density is 4.88 g/cm^3 for the sample mechanically alloyed for 3 h and sintered at 1150°C	The highest Ms value of 63.57 emu/g was measured for the sample mechanically alloyed for 3 h and sintered at 1150°C The highest coercivity, $H_{C'}$ value is 5.31 kOe obtained for the sample milled for 9 h and sintered at 900°C	[29]
$Ni_{0.3}Zn_{0.7}Fe_2O_4$	Sol–gel auto-combustion method	$Fe(NO_3)_3.9H_2O$ $Zn(NO_3)_2.4H_2O$ $Ni(NO_3)_2.6H_2O$	Sintering atmosphere: Air atmosphere Sintering temperature: 350, 400, 500, 600, 800, 1000 and 1200°C Sintering time: 1 h	Average crystallite sizes increased from 13.0 to 58 nm with increasing sintering temperatures	Highest M_s of 49.4 emu/g for sample sintered at 1200°C with the largest crystallite size Maximum H_c of13.82 Oe was observed in sample sintered at 800°C (crystallite size:36 nm) due to transition of the magnetic single-domain to magnetic multi-domain structure	[24]

http://dx.doi.org/10.5772/intechopen.68500

Material	Synthesis method	Starting materials	Sintering conditions	Microstructure features	Optimum magnetic properties	Reference
$Y_3Fe_5O_{12}$	Low temperature solid state reaction	$Y(NO_3)_3{\cdot}6H_2O$ $Fe(NO_3)_3{\cdot}9H_2O$ Citric acid	Sintering atmosphere: Air atmosphere Sintering temperatures: 1220, 1240, 1280 and 1320°C Sintering times: 3 h Heating rate:10°C/min	Optimum sintering temperature of 1280°C with highest value of ~5.08 g/cm^3 that was about 98% of the XRD density (5.17 g/cm^3)	M_s: 13.8 mT for sample sintered at 1280°C	[30]
$Mn_{0.49}Zn_{0.48}Fe_{2.06}O_4$	Co-precipitation method		Sintering atmosphere: air, mixture of nitrogen and air, and nitrogen atmospheres Sintering temperature: 850, 880, 900 and 950°C Heating rate: 5, 6, 7 and 8°C/min	Sintering in nitrogen produced pure $Mn_{0.49}Zn_{0.48}Fe_{2.06}O_4$ ferrite while sintered in air or mixture of air and nitrogen contained oxides such as Fe_2O_3, Mn_2O_3 and ZnO Highest sintering density of 4.82 g/cm^3 and homogeneous grain size were found in sample sintered at 880°C in nitrogen atmosphere with 5°C/min heating rate	Largest M_s value of 90.02 emu/g was observed in sample sintered at 880°C in nitrogen atmosphere with 5°C/min heating rate The M_s decreased with increasing heating rate from 90.02 to 80.60 emu/g	[22]
$Ni_{0.35}Cu_{0.05}Zn_{0.60}Fe_2O_4$ $Mg_{0.35}Cu_{0.05}Zn_{0.60}Fe_2O_4$	Conventional mixed oxide method and microwave sintering	NiO MgO CuO ZnO Fe_2O_3	Sintering temperature: 850, 875, 900, 925, 950, 975 and 1000°C Sintering time: 30 min	Largest grains and highest density of 5.28 and 4.95 g/cm^3 were observed in $Ni_{0.35}Cu_{0.05}Zn_{0.60}Fe_2O_4$ sintered at 950°C and $Mg_{0.35}Cu_{0.05}Zn_{0.60}Fe_2O_4$ sintered at 900°C, respectively	μ_i at 10 kHz showed maximum values of ~2825 for both $Ni_{0.35}Cu_{0.05}Zn_{0.60}Fe_2O_4$ sintered at 950°C and $Mg_{0.35}Cu_{0.05}Zn_{0.60}Fe_2O_4$ sintered at 900°C, respectively Highest M_s of ~129 and 88 emu/g for $Ni_{0.35}Cu_{0.05}Zn_{0.60}Fe_2O_4$ sintered at 950°C and $Mg_{0.35}Cu_{0.05}Zn_{0.60}Fe_2O_4$ sintered at 900°C, respectively	[31]

Material	Synthesis method	Starting materials	Sintering conditions	Microstructure features	Optimum magnetic properties	Reference
$Y_3Fe_5O_{12}$	Solid-state reaction method and microwave sintering	Fe_2O_3 Y_2O_3	**Conventional sintering (CS)** Sintering temperature: 1300°C Sintering time: 6 h Heating rate:2°C/min Cooling rate: 2°C/min **Microwave sintering (MS)** Sintering temperature: 900°C and 1000°C Sintering time: 20 min (for 900°C) and 30 min (for 1000°C) Heating rate: 8°C/min Cooling rate: 30°C/min	**Conventional sintering (CS)** Grain size: 3–5 μm Density: 98% T.D **Microwave sintering (MS)** Grain size: 1.5 μm (900°C), 5–10 μm (1000°C) Density: 96% T.D (900°C), 98% T.D (1000°C)	**Conventional sintering (CS)** M_s: 25.42 emu/g Coercive force, H_c: 25.36 Oe **Microwave sintering (MS)** M_s: 14.60 emu/g H_c: 34.82 Oe	[32]
$Mn_{1-x}Zn_xFe_2O_4$ (x = 0, 0.1, 0.2, 0.4)	Sol-gel combustion method	Fe_2O_3 SrO	Sintering atmosphere: Air atmosphere Sintering temperature: 700, 800 and 950°C Sintering time: 5 h	Average grain size: ~1–2 μm Density increased with increasing sintering temperatures from 4.64 to 4.80 g/cm^3	μ_i increased from 2100 to 2450 with increasing sintering temperatures. M_s: no sign of M_s even at 10000 Oe magnetic field	[33]

Table 1. Summary of synthesis methods, sintering conditions, microstructure features and optimum magnetic properties of ferrites.

http://dx.doi.org/10.5772/intechopen.68500

crystallite size is observed to be significantly increased with prolong sintering time up to 7 h [23], thus enhancing the saturation magnetization of the material. This may be as a result of the improved crystallinity, which implying a better exchange interaction.

However, the effects of sintering conditions, particularly sintering temperatures and times, on magnetic properties evolution are not necessarily increased with increase in sintering temperature or sintering time. This is attributed to the resulting microstructure features such as abnormal grains and pores which are related to the decrease of density, thus decreasing the magnetic properties, mainly the volume magnetization and the magnetic induction. The non-linear relationship is also due to the characteristic of the transition from single-domain to multi-domain grains. This phenomenon is largely observed in coercivity value against particle or grain size of the magnetic material [24].

6. Results from experimental works on single-sample sintering (SSS) and multi-sample sintering (MSS) of NiZn Ferrites and YIG

6.1. Comparative study of single-sample and multi-sample sintering of NiZn ferrites

Sintering temperatures increments from 600 to 1400°C increase the average grain size in both MSS and SSS as has been shown in **Table 2**, resulting from several processes. Those processes involve particles rearrangement and formation of dumbbell-liked structure between the particles contact points or known as the necking process. The grains are formed when the particles move closer during intermediate sintering stage as the sintering temperature goes higher. Finally, pores near or on the grain boundaries are gradually removed through the diffusion of vacancies associated by the pores along the grain boundaries, having only slight densification of the sample. The average grain size between the two different schemes shows small but significant difference. The striking difference in the microstructure is seen in $Ni_{0.3}Zn_{0.7}Fe_2O_4$ sintered at 1100°C as shown in **Figure 3(a)** and **(b)**. The striking difference arises from the

Sintering temperature (°C)		600	700	800	900	1000	1100	1200	1300	1400
Average grain size (μm)	MSS	0.19	0.21	0.23	0.24	0.43	1.07	1.23	2.65	4.98
	SSS	0.13	0.15	0.19	0.23	0.30	0.39	1.05	2.08	5.35
Experimental density (g/cm^3)	MSS	3.48	3.62	3.7	3.98	4.02	4.2	4.64	4.73	4.56
	SSS	4.23	4.49	4.62	4.73	4.78	4.81	4.91	4.93	4.88
Saturation induction, B_s (Gauss)	MSS	23.9	29.7	97.8	503.0	522.8	865.3	908.3	949.7	1076.0
	SSS	23.4	29.5	68.3	424.2	523.0	572.0	605.3	774.7	930.7
Coercivity, H_c (Oe)	MSS	3.4	7.7	12.5	5.0	4.1	1.3	1.2	0.5	0.4
	SSS	3.0	9.7	11.5	6.7	3.8	3.5	1.6	0.9	0.3

Table 2. Average grain size, experimental density, saturation induction and coercivity of $Ni_{0.3}Zn_{0.7}Fe_2O_4$ for different sintering temperatures.

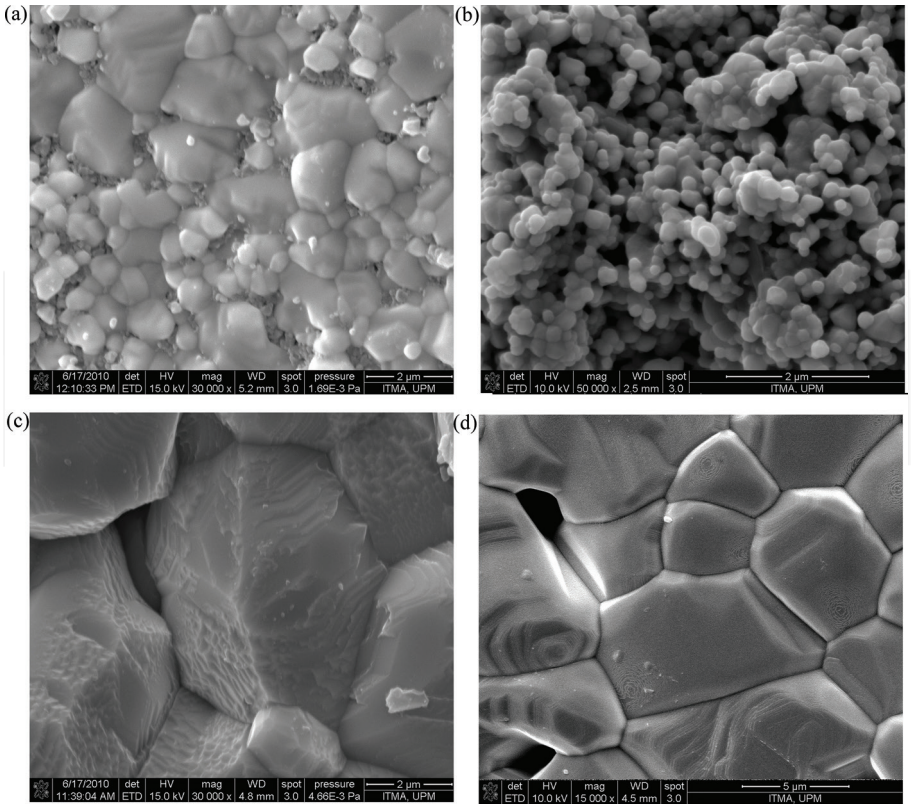

Figure 3. FESEM micrographs for $Ni_{0.3}Zn_{0.7}Fe_2O_4$ sintered at: (a) 1100°C (MSS), (b) 1100°C (SSS), (c) 1400°C (MSS) and (d) 1400°C (SSS).

different surface reactivities prior to the 1100°C sintering: for the MSS, the surface reactivity is high because the green bodies $Ni_{0.3}Zn_{0.7}Fe_2O_4$ are compacted from originally high-reactivity as-milled powders. However, the SSS is subjected to several times of repeated sintering, thus reducing the surface reactivity of the material prior to the 1100°C sintering. The pores which exist in MSS $Ni_{0.3}Zn_{0.7}Fe_2O_4$ sintered at 1400°C as shown in **Figure 3(c)** causing the decrease in density. Intragranular pores are trapped pores in the grains due to rapid grain growth and also probably due to zinc loss. The pores are known to be bad inclusions because they would pin down the domain wall, thus reducing the magnetization. However, no significant pores are observed in SSS $Ni_{0.3}Zn_{0.7}Fe_2O_4$ sintered at 1400°C. This is due to repeated sintering which could provide more time for the trapped pores to be removed; consequently, no significant amount of intragranular porosity was observed.

The focal question of what factors that subjected to different hysteresis shapes characteristic in both sintering treatments is of great interest. The shapes of the hysteresis loop are largely correlated with the microstructural features of the material, particularly the grains in the sample [34–40]. Besides, the disparities of the shapes also arise from the various grain shapes,

grain sizes, compositions, strains, and imperfections present in the sample. Maximum magnetic induction, B_s, of nickel zinc ferrite could range from 1000 to 3000 G [20, 41]. The experimental values of B_s are shown in **Table 2** range from 23.9 to 1076.0 G for MSS and from 23.4 to 930.7 G for SSS. The various ranges of B_s are subjected to the influence of several reasons in which categorizing the B-H hysteresis loops into several groups. The noticeably different B-H hysteresis loops are seen as three different shapes in both MSS and SSS. The loops are divided into three groups based on their magnetic behavior: strongly, moderately and weakly ferromagnetic, which are known to be strongly influenced by microstructural properties, domain states, and crystallinity of the samples. $Ni_{0.3}Zn_{0.7}Fe_2O_4$ sintered from 600 to 800°C for both MSS and SSS as shown in **Figure 4(a)** and **(b)**, respectively, is classified as the first group with weakly ferromagnetic behavior. The shape of the hysteresis loops is affected by mixture phases of ferromagnetic and paramagnetic phase and also most likely by some superparamagnetic phase [42]. The significant amount of amorphous grain boundary

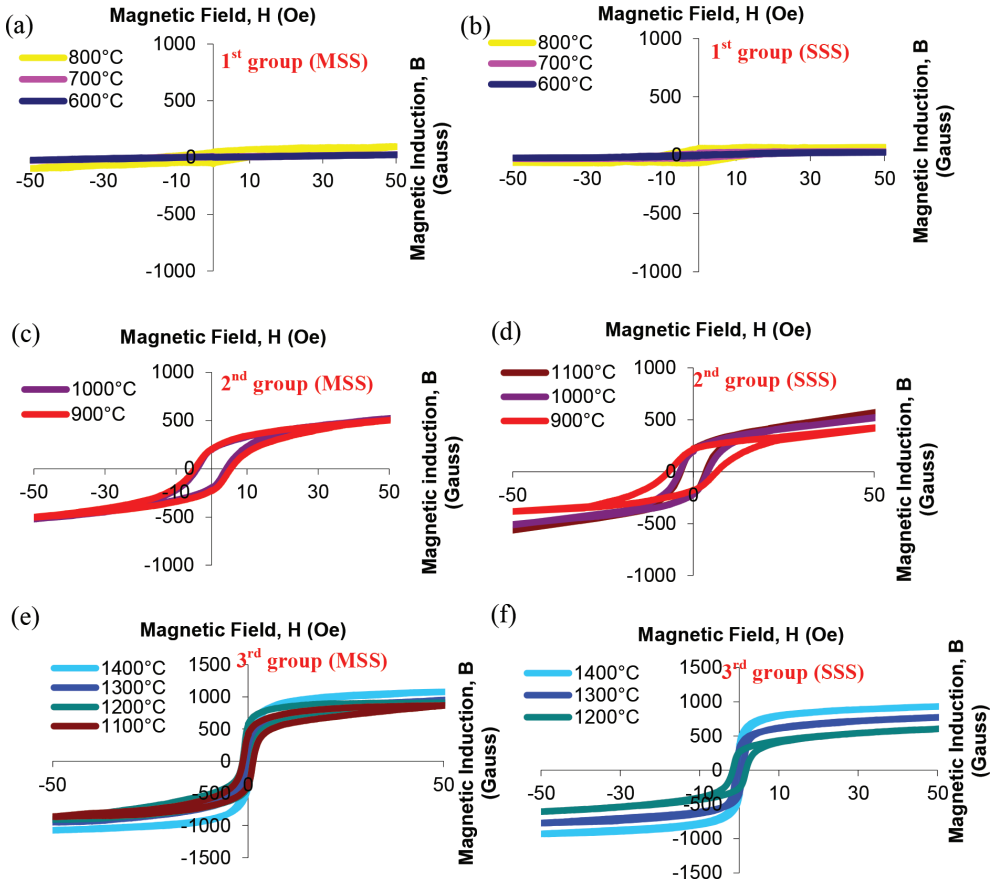

Figure 4. B-H hysteresis loops of $Ni_{0.3}Zn_{0.7}Fe_2O_4$ for first group of (a) MSS (b) SSS, second group of (c) MSS, (d) SSS, and third group of (e) MSS (f) SSS.

volumes has contributed to the paramagnetic phase, which arises from the fine grain size of the samples [36, 39, 42]. In addition, a superparamagnetic phase is contributed by the nano-sized grains. The shapes show a little hysteresis with narrowly bulging but linear-looking loops and have a very low Bs, indicating a very small amount of ferromagnetic phase. Due to the lower sintering temperature than the other two groups, the crystalline-phase percentage is small, while the amorphous-phase percentage is still significant. The grouping for the moderately ferromagnetic second group is slightly different between MSS and SSS where $Ni_{0.3}Zn_{0.7}Fe_2O_4$ sintered from 900 to 1000°C is for the MSS and from 900 to 1100°C is for SSS (see **Figures 4(c)** and **(d)**). The difference between the two sintering schemes is due to the influence of microstructural properties (see **Figure 3**). $Ni_{0.3}Zn_{0.7}Fe_2O_4$, which belongs to this group, shows a slanted sigmoid shape which is recognized to demonstrate moderate ferromagnetic behavior with negligible paramagnetic behavior since there is still remained a significant amount of the amorphous phase. The B-H loops of the MSS for this group have significantly higher B_s (M_s) values but falling Hc values (see **Figure 5**) indicating, respectively, higher ferromagnetic phase crystallinity and starting dominance of multi-domain magnetization-demagnetization processes. However, in the SSS, $Ni_{0.3}Zn_{0.7}Fe_2O_4$ still exhibits single domain grains as shown in **Figure 5**. Consequently, the magnetization of the SSS samples is largely exhibiting via spin rotation, thus lowering the magnetization values than that of MSS samples which already possessing multi-domain grains though sintered at similar sintering temperature. The result is clearly observed in $Ni_{0.3}Zn_{0.7}Fe_2O_4$ sintered at 1100°C: while the MSS sample already behaving as strongly ferromagnetic (third group), the SSS sample is still belong to the second group. The third group displays strongly ferromagnetic behavior (B_s, M_s) with a diminishing amorphous phase due to insignificant amount of amorphous grain boundaries volume. This behavior is exhibited by $Ni_{0.3}Zn_{0.7}Fe_2O_4$ sintered at much higher sintering temperature. The sintering temperatures range from 1100 to 1400°C for the MSS and from 1200 to 1400°C for the SSS. The well-known erect, narrower and well-defined sigmoid shape has been observed for the third group of hysteresis loops. This strongly ferromagnetic behavior is contributed by very high crystallinity, high density with a minute amount of microstructural defects, and large size of grains, resulting from high sintering temperature. Therefore, the combinations of these particular parameters would allow domain walls movement to become easier in the magnetization and demagnetization process.

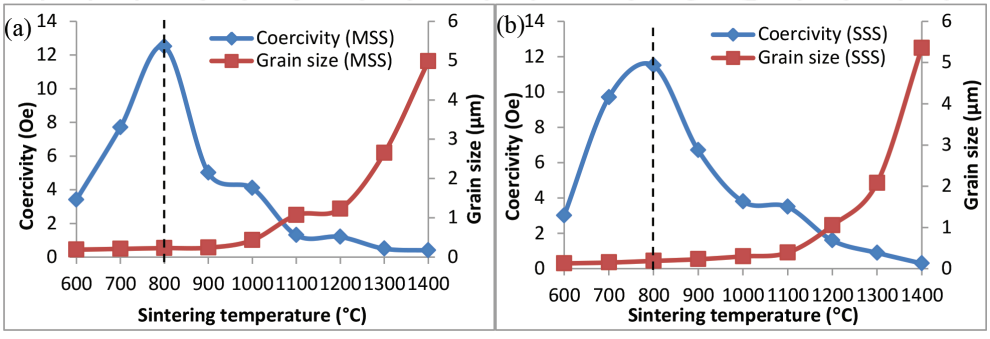

Figure 5. Coercivity and grain size as a function of sintering temperatures for (a) MSS and (b) SSS of $Ni_{0.3}Zn_{0.7}Fe_2O_4$ samples.

The H_c values in **Figures 5(a)** and **(b)** are found to increase as the sintering temperature increased from 600 to 800°C, reaches a maximum value and decreased from 800 to 1400°C. Interestingly, the similar trend is showed in both MSS and SSS schemes, proving the transition of single-domain to multi-domain grains happened in the similar grain size range. The drop of H_c values in SSS has occurred earlier for $Ni_{0.3}Zn_{0.7}Fe_2O_4$ having grain size of 0.19 μm as compared to MSS where it drops at 0.23 μm. H_c is probably the property most sensitive to porosity and grain size [20] nevertheless to the anisotropy field as well. Soft ferrites with nanometric grains exhibit a much higher H_c than samples having grain sizes of the order of few microns. An inversely proportional trend of H_c against grain size is observed for multi-domain grains, which consisting of more domain walls. Therefore, the contribution of lower energy domain walls movement to demagnetization or demagnetization than that of domain rotation increases. Consequently, coarse grains are expected to display low H_c [43]. However, below a certain size, which the H_c reaches a maximum value, or known as the critical size, the grains are single-domain grains [44, 45]. The increasing values of coercivity for lower sintering (≤800°C) were due to size-shape anisotropy (necking phase in the microstructure) and magnetocrystalline anisotropy. For higher sintering temperatures (≥900°C), the grain size exceeded the critical grain size with the disappearing size-shape anisotropy but with remaining magnetocrystalline anisotropy. Magnetocrystalline anisotropy is reduced in larger grains by decreasing the internal stress and crystal anisotropy [46], helping in better domain walls movement, thus decreasing the H_c. Within this grain size range, the anisotropy and defects including pores govern the H_c values. **Figure 5(a)** and **(b)** greatly affirms the trend, giving a maximum H_c of 12.5 Oe at 0.23 μm and 11.5 Oe 0.19 μm for MSS and SSS, respectively. Therefore, the range of critical size for $Ni_{0.3}Zn_{0.7}Fe_2O_4$ is approximately from 0.20 to 0.25 μm.

Figures 6 and **7** present the real part of permeability with frequency dispersion from 1 MHz to 1.8 GHz for both sintering schemes. Generally, the permeability is related to two different magnetizing mechanisms which are spin rotational and domain wall movement. Normally, spin rotation occurs at higher frequency when domain is damped and could not follow the applied electromagnetic wave. According to Snoek's law [47], the relation between resonance frequency f_R and the initial permeability μ_i for Ni–Zn ferrites may be expressed as follows:

$$f_R = (1/\mu_i) \times 3 \times 10^9 \text{ Hz} \quad (1)$$

This indicates that the lower the initial permeability values, the higher will be the frequency at which resonance phenomenon occurs. The value of real part of permeability for $Ni_{0.3}Zn_{0.7}Fe_2O_4$ sintered at 600 and 700°C for both sintering schemes is independent of frequency in this measured frequency region (1 MHz–1.8 GHz), whereas $Ni_{0.3}Zn_{0.7}Fe_2O_4$ sintered at 800°C only showed the dependency at about 100 MHz before reach the onset of resonance frequency. The resonance frequency is mostly observable in samples with lower sintering temperatures with the presence of single phase $Ni_{0.3}Zn_{0.7}Fe_2O_4$ (800–1000°C) for both sintering schemes. The coarsened grains for $Ni_{0.3}Zn_{0.7}Fe_2O_4$ sintered at 1100°C and above would lead to a ferromagnetic resonance at a lower frequency, in which, therefore, the resonance frequency could not be observed in the permeability spectra within the frequency region. At high frequencies, the domain walls cannot keep pace with the rapidly changing magnetic field, decreasing the value of real part of permeability. In powdered ferrites where each grain contains only a few domains, magnetization process occurs primarily by domain rotation and less by domain wall movement [48].

http://dx.doi.org/10.5772/intechopen.68500

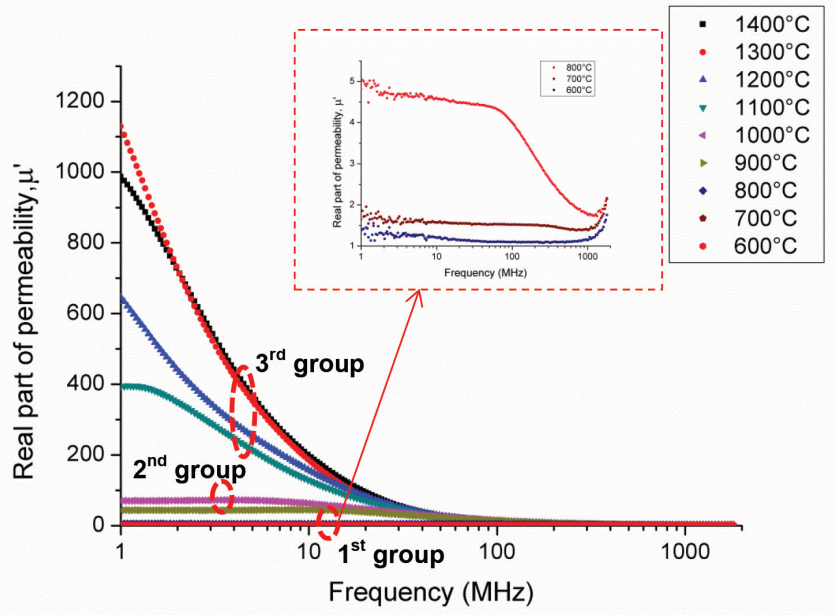

Figure 6. Graph of real permeability, μ′ against frequency for $Ni_{0.3}Zn_{0.7}Fe_2O_4$ multi-sample sintering.

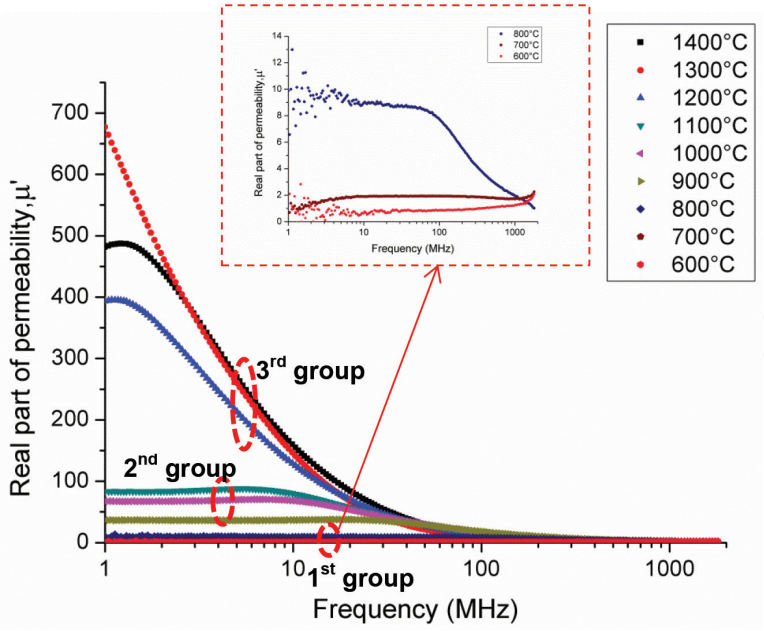

Figure 7. Graph of real permeability, μ′against frequency for $Ni_{0.3}Zn_{0.7}Fe_2O_4$ single-sample sintering.

The frequency stability for real permeability is varied from one group to another, which therefore varying the suitable applications for each group. The resonance frequency represents the high-frequency limit up to which the material can be used in a device. $Ni_{0.3}Zn_{0.7}Fe_2O_4$ with strong ferromagnetic behavior is suitable for lower frequency application (less than 1 MHz) because of the frequency stability at lower frequency where resonance frequency is found to be lowered than measured frequency range. Some applications that are operating in the frequency range of 0.5–5 MHz are ferrite antennas for medium and long wave broadcast bands, power transformers, and cores for electromagnetic suppression. For moderate ferromagnetic behavior, $Ni_{0.3}Zn_{0.7}Fe_2O_4$ sintered through MSS displays ferromagnetic resonance at frequency of 10.7 MHz (sintered at 900°C) and 3.9 MHz (sintered at 1000°C) with maximum real part of permeability value of 44.4 and 72.1, respectively, whereas for $Ni_{0.3}Zn_{0.7}Fe_2O_4$ sintered through SSS, samples demonstrate ferromagnetic resonance at frequency of 20.1 MHz (sintered at 900°C), 6.31 MHz (sintered at 1000°C), 5.40 MHz (sintered at 1100°C) with maximum real part of permeability value of 37.4, 70.5 and 87.9, respectively. The materials could be used for the application of the solid core of inductors for resonant circuits or transformers operating in the approximate frequency range 2–20 MHz [41, 49], ferrite antennas for short wave broadcast bands, power transformers for the approximate frequency range 2–30 MHz and cores for electromagnetic interference suppression [41]. For weak ferromagnetic behavior, only $Ni_{0.3}Zn_{0.7}Fe_2O_4$ sintered at 800°C for both sintering schemes displays the resonance phenomenon. The frequencies are stabled until 44.3 and 39.5 MHz for SSS and MSS, respectively, with maximum real part of permeability value of 8.64 and 4.42, respectively. Permeability with a value less than 12 is used for inductors and for resonant circuits operating at frequencies above 30 MHz and cores for electromagnetic interference suppression, whereas a much higher frequency than 1.8 GHz is needed to show resonance behavior in $Ni_{0.3}Zn_{0.7}Fe_2O_4$ sintered at 600 and 700°C due to smaller grain size and lower magnetic mass in the $Ni_{0.3}Zn_{0.7}Fe_2O_4$.

The complex permeability could also be classified into three different groups which are value-differentiated groups: strongly, moderately and weakly ferromagnetic behavior. By determining the critical size of single-domain to multi-domain grains through plot in **Figure 5**, it is found that $Ni_{0.3}Zn_{0.7}Fe_2O_4$ with weakly ferromagnetic behavior contains less than 50% multi-domain grains ($Ni_{0.3}Zn_{0.7}Fe_2O_4$ sintered from 600 to 800°C for MSS and SSS), whereas $Ni_{0.3}Zn_{0.7}Fe_2O_4$ with the moderately ferromagnetic behavior possesses more than 50% multi-domain grains ($Ni_{0.3}Zn_{0.7}Fe_2O_4$ sintered from 900 to 1000°C for MSS; $Ni_{0.3}Zn_{0.7}Fe_2O_4$ sintered from 900 to 1100°C for SSS), and 100% of the grains are multi-domain grains ($Ni_{0.3}Zn_{0.7}Fe_2O_4$ sintered from 1100 to 1400°C for MSS; $Ni_{0.3}Zn_{0.7}Fe_2O_4$ sintered from 1200 to 1400°C for SSS) which are counted as strongly ferromagnetic behavior. Therefore, $Ni_{0.3}Zn_{0.7}Fe_2O_4$ sintered below 800°C (with grain size less than 0.25 μm) is dominated by spin rotation, whereas $Ni_{0.3}Zn_{0.7}Fe_2O_4$ sintered from 800°C upwards dominated by domain wall movement and spin rotation. The reason for the increase in permeability with sintering temperature is attributed to the increase of grain size and reduction of porosity, reducing the anisotropy arising from the demagnetizing fields outside of grains. Fewer number of the grain boundaries would be present in $Ni_{0.3}Zn_{0.7}Fe_2O_4$ sintered at high temperatures, causing the existence of very mobile domain walls thus increasing the permeability value. Moreover, during grain growth, many pores would be removed, thus reducing the hindrance to the domain walls motion because pores provide stress concentration that may affect the magnetization's easy direction. However, the decrease in the real part of the permeability for $Ni_{0.3}Zn_{0.7}Fe_2O_4$ sintered at 1400°C is attributed to zinc loss [47] and existence of pores (see **Figure 3**).

The loss factor is observed to increase with a rise of the frequency from 1 MHz and attain the maximum value at a particular frequency and decreased with a further increase in frequency. The loss factor values increase with increasing sintering temperature in both MSS and SSS as shown in **Figures 8** and **9** for MSS and SSS, respectively. The frequency at which losses begin to increase due to the onset of resonance varies with the sintering temperatures from 2 to 100 MHz for both sintering schemes. As the sintering temperatures increase, the domain walls movement becomes easier in the larger grain, thus inducing larger eddy current. It is caused by the changing magnetic fields inside the sample which give rise to circulating currents inside the sample, and hence to energy losses [50]. However, in $Ni_{0.3}Zn_{0.7}Fe_2O_4$, eddy current losses are not dominant due to its high electrical resistivity. The larger grain raises the number and size of magnetic domains which contribute to loss due to delay in domain wall motion. The losses in ferrites are associated with domain wall relaxation and rotational resonance. In higher frequency regions (>500 MHz), most of the domain walls are damped and become less important as spin rotational would continue to occur [20].

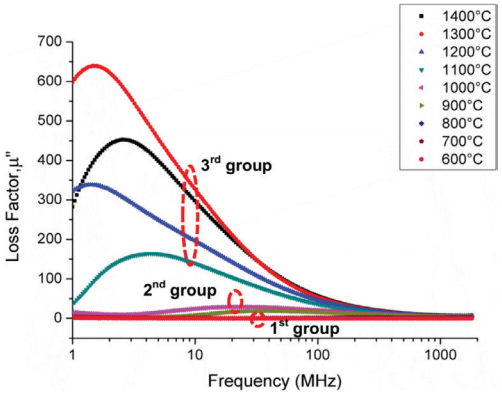

Figure 8. Graph of loss factor, μ″ against frequency for $Ni_{0.3}Zn_{0.7}Fe_2O_4$ multi-sample sintering.

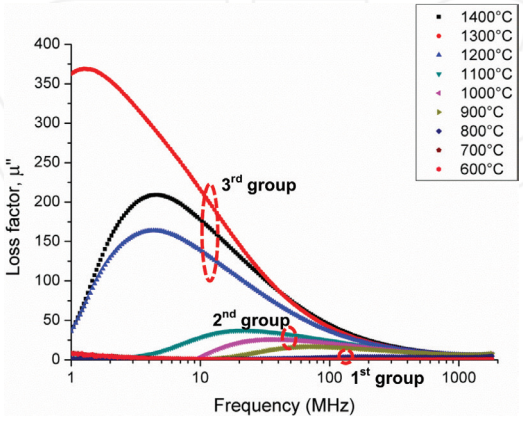

Figure 9. Graph of loss factor, μ″ against frequency for $Ni_{0.3}Zn_{0.7}Fe_2O_4$ single-sample sintering.

6.2. Comparative study of single-sample and multi-sample sintering of yttrium iron garnet

A systematic track of microstructure-magnetic properties evolution of several polycrystalline Yttrium iron garnet (YIG) ferrite samples as a result of different sintering schemes was investigated in detail, focusing on the attendant occurrence of their dependency: an aspect seemingly ignored, hitherto in the garnet ferrite previous literatures for the past eight decades.

In order to prepare Yttrium iron garnet (YIG) ferrite sample, Fe_2O_3 (Alfa Aesar, 99.945%) and Y_2O_3 (Alfa Aesar, 99.99%) powders were weighed and mixed according to the stoichiometric proportions required in the final YIG samples based on the reaction:

$$3Y_2O_3 + 5Fe_2O_3 \rightarrow 2Y_3Fe_5O_{12} \quad (2)$$

The powder then mechanically alloyed into nanosize via mechanical alloying technique. Two batches of samples were produced with different sintering scheme: SSS and MSS, each covering a range of low sintering temperature from 600°C up to high sintering temperature of 1400°C with 100°C increments. The samples were analyzed by using a LEO 912AB energy filter transmission electron microscope (TEM), Philips Expert PW3040 diffractometer operating at 40 kV/30 mA using Cu Kα radiation, scanning electron microscopy (SEM), MATS-2010S Static Hysteresis Graph at room temperature under applied magnetic fields 0–50 Oe (0–4000 A/m) and HP4291B Materials Impedance Analyzer at room temperature for their evolution stage in crystalline phases, microstructure, magnetic hysteresis-loop parameters, and magnetic permeability components, respectively.

With great experimental care, both the SSS and MSS batches yielded similar variation of microstructure-magnetic properties evolution (**Table 3**). The results showed an increasing tendency of

Sintering temperature, (T, °C)	Single-sample sintering				Multi-sample sintering			
	Grain size, (±0.01 μm)	Saturation induction, B_s (Gauss)	Saturation magnetization, M_s (emu/cm^3)	Coercivity, H_c (Oe)	Grain size, (±0.01 μm)	Saturation induction, B_s (Gauss)	Saturation magnetization, Ms (emu/cm^3)	Coercivity, H_c (Oe)
600	0.16	2.1	1.7	2.6	0.20	16.9	2.2	0.1
700	0.17	2.3	2.6	3.1	0.21	24.9	2.7	0.7
800	0.18	16.4	3.9	6.7	0.25	35.8	4.7	1.3
900	0.28	20.6	4.8	10.9	0.26	49.6	5.2	3.9
1000	0.33	120.7	5.4	15.5	0.28	128.6	5.5	15.8
1100	0.60	173.2	5.7	18.5	0.58	185.7	6.2	19.3
1200	1.14	223.7	10.9	12.4	0.80	244.5	12.8	15.2
1300	1.68	378.9	21.2	7.4	1.25	463.1	23.3	8.8
1400	2.71	570.4	26.3	4.3	3.09	714.6	29.1	2.9

Table 3. Microstructural and magnetic parameters of single- and multi-sample sintering YIG samples with various sintering temperature variations.

the saturation magnetization and magnetic induction with grain size, which was attributed to increase of crystallinity and demagnetizing field reduction in the grains. The variation in coercivity corresponded to the changes of anisotropy field within the samples due to grain size changes. Specifically, the starting appearance of room temperature ferromagnetic order suggested by the sigmoid-shaped B-H loops seems to be dependent on a sufficient number of large enough magnetic-domain containing grains formed in the microstructure. Viewed simultaneously, the B-H loops (appeared to be belonging to three groups with different magnetism-type dominance, respectively dependent on phase purity and distribution of grain size. The clearly tracked evolution of the hysteresis (**Figures 10** and **11**) and permeability component (**Figure 12**) strongly suggests that high reactivity grain surfaces and great-care human handling of the sample preparation process contributed to the startlingly clear microstructure-property evolution trends.

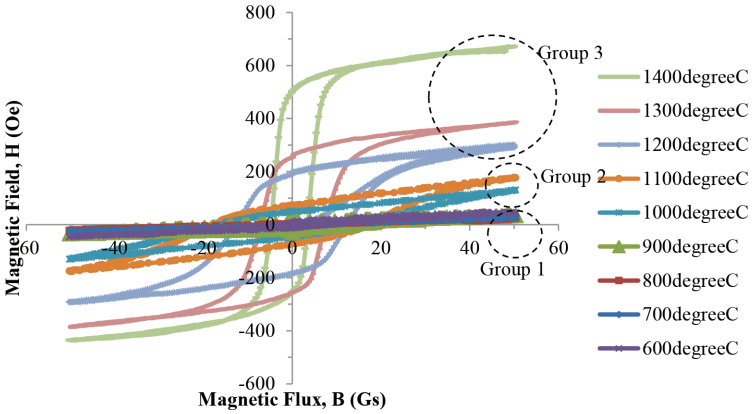

Figure 10. B-H hysteresis loop for single-samples sintered at various temperatures. The circles inside the figure indicate 3 different groups of B-H curve evolution.

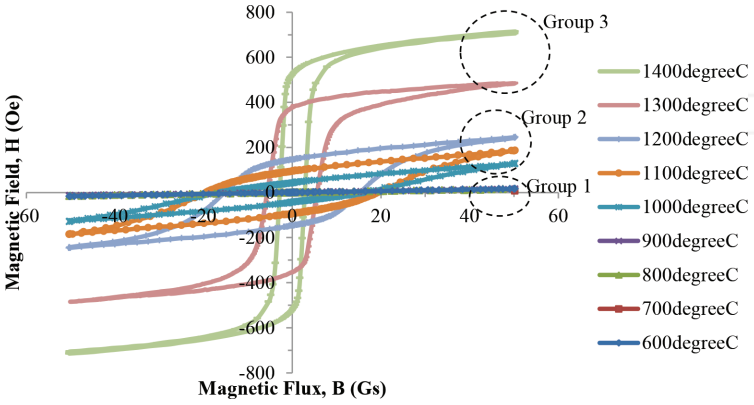

Figure 11. B-H hysteresis loop for multi-samples sintered at various temperatures. The circles inside the figure indicate 3 different groups of B-H curve evolution.

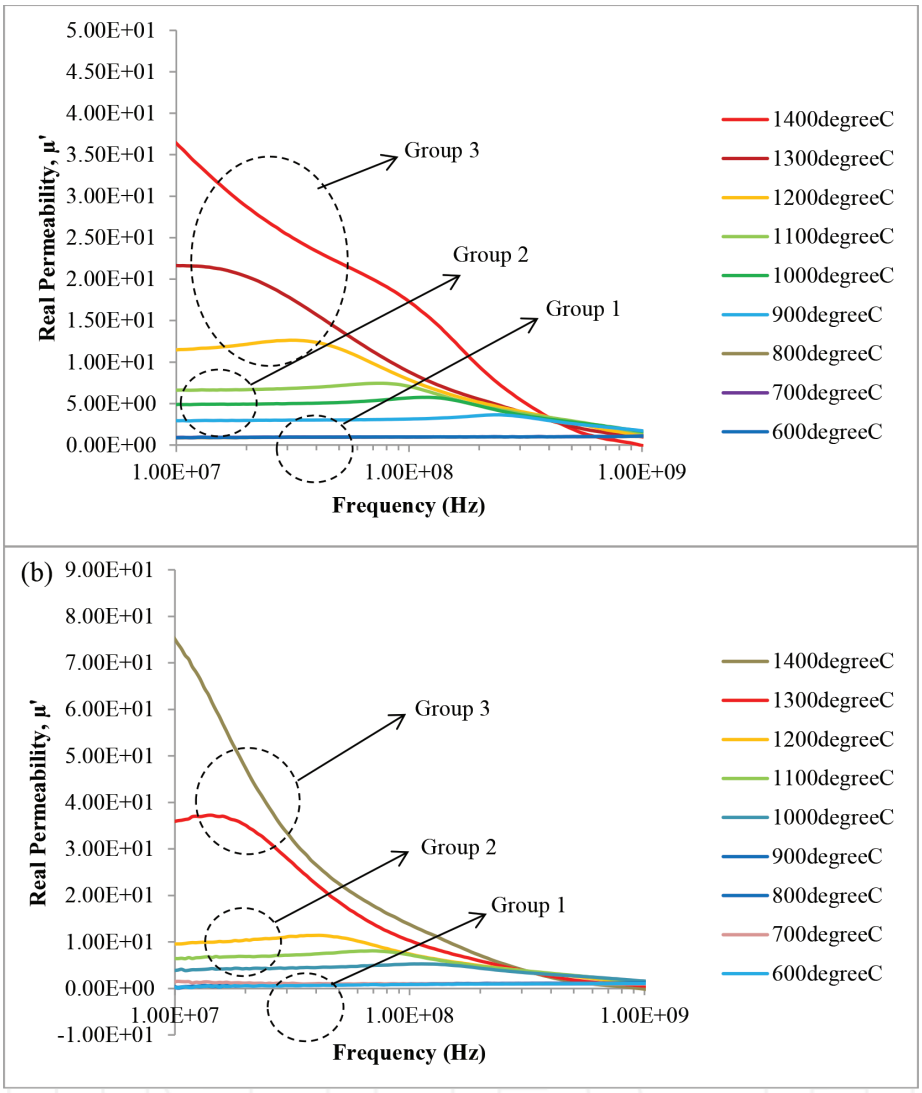

Figure 12. Real permeability measured at room temperature in range 10 MHz to 1 GHz (a) single-sample sintering; (b) multi-samples sintering samples.

Acknowledgements

We would like to dedicate this chapter and show our gratitude to the late Assoc. Prof. Dr. Mansor Hashim from Universiti Putra Malaysia, Malaysia for sharing his pearls of wisdom with us during the course of this research.

Author details

Ismayadi Ismail[1]*, Idza Riati Ibrahim[1] and Rodziah Nazlan[2]

*Address all correspondence to: ismayadi@upm.edu.my

1 Materials Synthesis and Characterisation Laboratory, Institute of Advanced Technology, Universiti Putra Malaysia, Serdang, Selangor, Malaysia

2 Department of Material Technology, Faculty of Industrial Science and Technology, Universiti Malaysia Pahang, Kuantan, Pahang, Malaysia

References

[1] Cao G, Wang Y. Nanostructures and Nanomaterials: Synthesis, Properties, and Applications. 2nd ed. Toh Tuck Lin: World Scientific. 2011

[2] Winterer M. Nanocrystalline Ceramics Synthesis and Structure. New York: Springer-Verlag Berlin Heidelberg. 2002

[3] Yan YI, Ngo KDT, Hou D, Mu M, Mei Y, Lu G. Effect of sintering temperature on magnetic core-loss properties of a NiCuZn ferrite for high-frequency power converters. Journal of Electronic Materials. 2015;**44**(10):3788-3794. DOI: 10.1007/s11664-015-3836-z

[4] Rana K, Thakur P, Sharma P, Tomar M, Gupta V, Thakur A. Improved structural and magnetic properties of cobalt nanoferrites : Influence of sintering temperature. Ceramics International. 2015;**41**:4492-4497. DOI: http://dx.doi.org/10.1016/j.ceramint.2014.11.143

[5] Huang CC, Hung YH, Huang JY, Kuo MF. Impact of stoichiometry and sintering temperature on magnetic properties of $Y_3Mn_xAl_{0.83-x}Fe_{4.17}O_{12}$ ferrites. IEEE Transactions on Magnetics. 2014;**50**(8):5-8. DOI: 10.1109/TMAG.2014.2310703

[6] Sujatha C, Reddy KV, Babu KS, Reddy AR, Rao KH. Effect of sintering temperature on electromagnetic properties of NiCuZn ferrite. Ceramics International. 2013;**39**(3):3077-3086. DOI: http://dx.doi.org/10.1016/j.ceramint.2012.09.087

[7] Islam R, Rahman O, Hakim MA, Saha DK. Effect of Sintering. Temperature on structural and magnetic properties of $Ni_{0.55}Zn_{0.45}Fe_2O_4$ ferrites. Materials Sciences and Applications. 2012;**3**:326-331. DOI: http://dx.doi.org/10.4236/msa.2012.35048

[8] Shirsath SE, Kadam RH, Gaikwad AS, Ghasemi A, Morisako A. Effect of sintering temperature and the particle size on the structural and magnetic properties of nanocrystalline $Li_{0.5}Fe_{2.5}O_4$. Journal of Magnetism and Magnetic Materials. 2011;**323**:3104-3108. DOI: http://dx.doi.org/10.1016/j.jmmm.2011.06.065

[9] Liu C, Lan Z, Jiang X, Yu Z, Sun K, Li L, et al. Effects of sintering temperature and Bi_2O_3 content on microstructure and magnetic properties of LiZn ferrites. Journal of Magnetism and Magnetic Materials. 2008;**320**:1335-1339. DOI: http://dx.doi.org/10.1016/j.jmmm.2007.10.016

[10] Kingery WD, Bowen HK, Uhlmann DR. Introduction to Ceramics. 2nd ed. New York: John Wiley & Sons Limited. 1976

[11] Tan W, Cuellar C, Margueron X, Idir N. A common-mode choke using Toroid-EQ mixed structure. IEEE Transactions on Power Electronics. 2013;**28**(1):31-35. DOI: 10.1109/TPEL.2012.2205708

[12] Waqas H, Hussain A, Muhammad Q. Effect of firing temperature on the electromagnetic properties of electronic transformer cores developed by using Nanosized Mn–Zn Ferrite powders. Acta Metallurgica Sinica (English Letters). 2015;**28**(2):159-163. DOI: 10.1007/s40195-014-0180-x

[13] Mcdonald T. Design and characterization of a miniature varactor tuned ferrite rod antenna for 4 to 24 MHz. In: 2013 Loughborough Antennas & Propagation Conference. IEEE. 2013. pp. 250-254

[14] Dar MA, Majid K, Hanief M, Kotnala RK, Shah J. Synthesis and characterization of Li0.5Fe2.5-xGdxO4 ferrite nano-particles as a potential candidate for microwave device applications. Materials and Design. 2016;**90**:443-452. DOI: http://dx.doi.org/10.1016/j.matdes.2015.10.151

[15] Ramesh T, Shinde RS, Murthy SR. Synthesis and characterization of nanocrystalline $Ni_{0.94}Co_{0.03}Mn_{0.04}Cu_{0.03}Fe_{1.96-x}Al_xO_4$ ferrites for microwave device applications. Journal of Magnetism and Magnetic Materials. 2013;**345**:276-281. DOI: http://dx.doi.org/10.1016/j.jmmm.2013.06.041

[16] Cheng YJ, Member S, Huang QD, Wang YR, Li JL. Narrowband substrate integrated waveguide isolators. IEEE Microwave and Wireless Component Letters 2014;**24**(10):698-700. DOI: 10.1109/LMWC.2014.2344440

[17] Geiler AL, Harris VG. Atom magnetism: Ferrite circulators—past, present, and future. IEEE Microwave Magazine. 2014;**15**(6):66-72. DOI: 10.1109/MMM.2014.2332411

[18] Yang X, Wu J, Gao Y, Nan T, Zhou Z, Beguhn S, Liu M, Sun NX. Compact and low loss phase shifter with low bias field using partially magnetized ferrite. IEEE Transactions on Magnetics. 2013;**49**(7):3882-3885. DOI: 10.1109/TMAG.2013.2244860

[19] Goldman A. Handbook of Modern Ferromagnetic Materials. Massachusetts: Kluwer Academic Publishers. 1999

[20] Goldman A. Modern Ferrite Technology. Pittsburgh: Springer Science and Business Media, Inc. 2006

[21] Gholizadeh A, Jafari E. Effects of sintering atmosphere and temperature on structural and magnetic properties of Ni-Cu-Zn ferrite nano-particles: Magnetic enhancement by a reducing atmosphere. Journal of Magnetism and Magnetic Materials. 2017;**422**:328-336. DOI: http://dx.doi.org/10.1016/j.jmmm.2016.09.029

[22] Wang GX, Wu HX, Jiang YF, Peng HF, Wang X. Effect of sintering conditions on the properties of Mn-Zn Ferrites produced by Co-precipitation. Advanced Materials Research. 2011;**391-392**:839-843. DOI: 10.4028/www.scientific.net/AMR.391-392.839

[23] Sun K, Liu H, Yang Y, Yu Z, Chen C, Wu G, Jiang X, Lan Z, Li L. Contribution of magnetization mechanisms in nickel-zinc ferrites with different grain sizes and its temperature relationship. Materials Chemistry and Physics. 2016;**175**:131-137. DOI: http://dx.doi.org/10.1016/j.matchemphys.2016.03.002

[24] Rahimi M, Kameli P, Ranjbar M, Salamati H. The effect of sintering temperature on evolution of structural and magnetic properties of nanostructured $Ni_{0.3}Zn_{0.7}Fe_2O_4$ ferrite. Journal of Nanoparticle Reseacrh. 2013;**15**:1865-1876. DOI: 10.1007/s11051-013-1865-1

[25] Sun L, Zhang R, Wang Z, Ju L, Cao E, Zhang Y. Structural, dielectric and magnetic properties of $NiFe_2O_4$ prepared via sol-gel auto-combustion method. Journal of Magnetism and Magnetic Materials. 2017;**421**:65-70. DOI: http://dx.doi.org/10.1016/j.jmmm.2016.08.003

[26] Thakur A, Kumar P, Thakur P, Rana K, Chevalier A, Mattei JL, et al.: Enhancement of magnetic properties of Ni0.5Zn0.5Fe_2O_4 nanoparticles prepared by the co-precipitation method. Ceramics International. 2016;**42**(9):10664-10670. DOI: http://dx.doi.org/10.1016/j.ceramint.2016.03.173

[27] Li XX, Zhou JJ, Deng JX, Zheng H, Zheng L, Zheng P, Qin HB. Synthesis of dense, fine-grained YIG ceramics by two-step sintering. Journal of Electronic Materials. 2016;**45**(10):4973-4978. DOI: 10.1007/s11664-016-4690-3

[28] Ghodake JS, Shinde TJ, Patil RP, Patil SB, Suryavanshi SS: Initial permeability of Zn-Ni-Co ferrite. Journal of Magnetism and Magnetic Materials. 2015;**378**:436-439. DOI: http://dx.doi.org/10.1016/j.jmmm.2014.11.041

[29] Sadullahoglu G, Ertug B, Gökçe H, Altuncevahir B, Öztürk M, Topkaya R, Akdogan N, Öveçoglu ML, Addemir O. The effect of milling time and sintering temperature on crystallization of $BaFe_{12}O_{19}$ phase and magnetic properties of Ba-hexaferrite magnet. Acta Physica Polonica A. 2015;**128**(3):377-382. DOI: dx.doi.org/10.12693/APhysPolA.128.377

[30] Yu H, Zeng L, Lu C, Zhang W, Xu G. Synthesis of nanocrystalline yttrium iron garnet by low temperature solid state reaction. Materials Characterization. 2011;**62**(4):378-381. DOI: http://dx.doi.org/10.1016/j.matchar.2011.02.002

[31] Penchal Reddy M, Madhuri W, Venkata Ramana M, Ramamanohar Reddy N, Siva Kumar K V., Murthy VRK, Siva Kumar K, Ramakrishna Reddy R. Effect of sintering temperature on structural and magnetic properties of NiCuZn and MgCuZn ferrites. Journal of Magnetism and Magnetic Materials. 2010;**322**(19):2819-2823. DOI: http://dx.doi.org/10.1016/j.jmmm.2010.04.036

[32] Yang Q, Zhang H, Liu Y, Wen Q, Jia L. The magnetic and dielectric properties of microwave sintered yttrium iron garnet (YIG). Materials Letters. 2008;**62**(17-18):2647-2650. DOI: 10.1016/j.matlet.2008.01.040

[33] Azadmanjiri J: Preparation of Mn—Zn ferrite nanoparticles from chemical sol—gel combustion method and the magnetic properties after sintering. Journal of Non-Crystalline Solids. 2007;**353**:4170-4173. DOI: 10.1016/j.jnoncrysol.2007.06.046

[34] Nazlan R, Hashim M, Ibrahim IR, Idris FM, Wan Ab Rahman WN, Abdullah NH, Ismail I, Kanagesan S, Abbas Z, Azis RS. Influence of indium substitution and microstructure

changes on the magnetic properties evolution of $Y_3Fe_{5-x}In_xO_{12}$. Journal of Materials Science: Materials in Electronics. 2015;**26**(6):3596-3609. DOI: 10.1007/s10854-015-2874-x

[35] Low ZH, Hashim M, Ismail I, Kanagesan S, Shafie MSE, Mohd Idris F, Ibrahim IR. Development of magnetic B-H hysteresis loops through stages of microstructure evolution of bulk $BaFe_{12}O_{19}$. Journal of Superconductivity and Novel Magnetism. 2015;**28**:3075-3086. DOI: 10.1007/s10948-015-3099-1

[36] Shafie MSE, Hashim M, Ismail I, Kanagesan S, Fadzidah MI, Idza IR, Hajalilou A, Sabbaghizadeh R. Magnetic M–H loops family characteristics in the microstructure evolution of $BaFe_{12}O_{19}$. Journal of Materials Science: Materials in Electronics. 2014;**25**(9):3787-3794. DOI: 10.1007/s10854-014-2090-0

[37] Ibrahim IR, Hashim M, Nazlan R, Ismail I, Kanagesan S, Wan Ab Rahman WN, Abdullah NH, Mohd Idris F, Bahmanrokh G. A comparative study of different sintering routes effects on evolving microstructure and B–H magnetic hysteresis in mechanically-alloyed Ni–Zn ferrite, $Ni_{0.3}Zn_{0.7}Fe_2O_4$. Journal of Materials Science: Materials in Electronics. 2014;**26**(1):59-65. DOI: 10.1007/s10854-014-2362-8

[38] Ismail I, Hashim M, Kanagesan S, Ibrahim IR, Nazlan R, Wan Ab Rahman WN, Abdullah NH, Mohd Idris F, Bahmanrokh G, Shafie MSE, Manap M. Evolving microstructure, magnetic properties and phase transition in a mechanically alloyed $Ni_{0.5}Zn_{0.5}Fe_2O_4$ single sample. Journal of Magnetism and Magnetic Materials. 2014;**351**:16-24. DOI: dx.doi.org/10.1016/j.jmmm.2013.09.041

[39] Nazlan R, Hashim M, Ibrahim IR, Ismail I. Dependence of magnetic hysteresis on evolving Single-Sample sintering in fine-grained Yttrium iron garnet. Journal of Superconductivity and Novel Magnetism. 2013;**27**(2):631-639. DOI: 10.1007/s10948-013-2328-8

[40] Bean CP. Hysteresis loops of mixtures of ferromagnetic micropowders. Journal of Applied Physics. 1955;**26**:1381-1383. DOI: http://dx.doi.org/10.1063/1.1721912

[41] Snelling EC. Soft ferrites: Properties and Applications. Massachusetts: Butterworths Publishing. 1985

[42] Ibrahim IR, Hashim M, Nazlan R, Ismail I, Wan Ab Rahman WN. Influence of evolving microstructure on magnetic-hysteresis characteristics in polycrystalline nickel–zinc ferrite, $Ni_{0.3}Zn_{0.7}Fe_2O_4$. Materials Research Bulletin. 2012;**47**(6):1345-1352. DOI: 10.1016/j.materresbull.2012.03.007

[43] Jahanbin T, Hashim M, Matori KA, Waje SB. Influence of sintering temperature on the structural, magnetic and dielectric properties of $Ni_{0.8}Zn_{0.2}Fe_2O_4$ synthesized by co-precipitation route. Journal of Alloys and Compounds. 2010;**503**(1):111-117. DOI: http://dx.doi.org/10.1016/j.jallcom.2010.04.212

[44] Azizi A, Sadrnezhaad SK. Effects of annealing on phase evolution, microstructure and magnetic properties of mechanically synthesized nickel-ferrite. Ceramics International. 2010;**36**(7):2241-2245. DOI: http://dx.doi.org/10.1016/j.ceramint.2010.06.004

[45] George M, John AM, Nair, S. S., Joy PA, Anantharaman MR. Finite size effects on the structural and magnetic properties of sol–gel synthesized $NiFe_2O_4$ powders. Journal of Magnetism and Magnetic Materials. 2006;**302**(1):190-195. DOI: http://dx.doi.org/10.1016/j.jmmm.2005.08.029

[46] Verma A, Goel TC, Mendiratta RG. Frequency variation of initial permeability of NiZn ferrites prepared by the citrate precursor method. Journal of Magnetism and Magnetic Materials. 2000;**210**:274-278. DOI: http://dx.doi.org/10.1016/S0304-8853(99)00451-5

[47] Nakamura T. Low-temperature sintering of Ni–Zn–Cu ferrite and its permeability spectra. Journal of Magnetism and Magnetic Materials. 1997;**168**:285-291. DOI: http://dx.doi.org/10.1016/S0304-8853(96)00709-3

[48] Naughton BT, Majewski P, Clarke DR. Magnetic properties ofnickel–zinc ferrite toroids prepared from nanoparticles. Journal of American Ceramic Society. 2007;**90**:3547-3553. DOI: 10.1111/j.1551-2916.2007.01981.x

[49] Warne DF. Newnes Electrical Power Engineer's Handbook. 2nd ed. Oxford: Elsevier Publications. 2005

[50] Jahanbin T, Hashim M, Matori KA. Comparative studies on the structure and electromagnetic properties of Ni–Zn ferrites prepared via co-precipitation and conventional ceramic processing routes. Journal of Magnetism and Magnetic Materials. 2010;**322**(18):2684-2689. DOI: http://dx.doi.org/10.1016/j.jmmm.2010.04.008

INTECH